*Progress in Propulsion Physics* **11** (2019) 273-294
https://doi.org/10.1051/eucass/201911273

# ONE-DIMENSIONAL MODEL DESCRIBING EIGENMODE FREQUENCY SHIFT DURING TRANSVERSE EXCITATION

**S. Webster, J. Hardi, and M. Oschwald**

German Aerospace Center (DLR), Lampoldshausen
Im Langen Grund, Hardthausen 74239, Germany

A shift in transverse eigenmode frequency was observed in an experimental combustion chamber when exposed to large amplitude acoustic oscillations during oxygen–hydrogen combustion tests. A shift in eigenmode frequency under acoustic conditions representative of combustion conditions is of critical importance when tuning acoustic absorbers or investigating injection coupled combustion instabilities. The experimentally observed frequency shift was observed both in the frequency domain and as an asymmetric amplitude response to a linear frequency ramp of an external excitation system in the time domain. The frequency shift was found to be dependent on amplitude and operating condition. A hypothesis is presented for the frequency shift based on change in speed-of-sound distributions due to flame contraction when exposed to high amplitude pressure oscillations. A one-dimensional (1D) model was created to test the hypothesis. Model parameters were based on relationships observed in experimental data. The model was found to accurately recreate the frequency shifting asymmetric response observed in test data as well as its amplitude dependence. Further development is required to investigate the influence of operating conditions and chamber design on the quantitative modeling of the frequency shift.

## 1 INTRODUCTION

High-frequency (HF) combustion instabilities are an ongoing challenge to rocket development programs. Significant progress in understanding has been made since combustion instabilities were first identified in the 1940s. However, due to the complicated processes present during rocket combustion, further research of the physical process that leads to combustion instabilities as well as development of tools to predict and limit the risk of combustion instabilities are still required [1].

High-frequency combustion instability occurs when combustion processes couple with the local acoustic field and is characterized by high-amplitude pressure oscillations that can lead to the rapid degradation of the rocket combustion chamber [2]. The frequency of the pressure oscillations is defined by the speed-of-sound and the combustion chamber geometry and is of critical importance when analyzing coupling as both injector resonance coupling and combustion chamber processes have been shown to be sensitive to oscillation frequency [3].

Investigation and identification of acoustic eigenmode frequencies can be made both experimentally and numerically [4, 5]. Analytical or numerical calculations which assume a constant speed-of-sound are limited in accuracy. Analysis presented in [6] identified frequency shifts in the first transverse eigenmode (1T mode) based on axial position in the combustion chamber. Using the PIANO-SAT acoustic simulation software, the difference in frequency was identified as originating from a nonuniform speed of sound distribution in the combustion chamber. This highlighted the importance of using a representative speed-of-sound distribution for accurate prediction of eigenmode frequencies under combustion conditions.

In a coaxial injection system, the length of the central liquid oxygen (LOx) jet has been shown to be highly dependent on acoustic amplitude [7]. When exposed to high acoustic amplitudes, the flame contracts toward the injection plane leading to increased heat loads to the wall and the injection plate. Injection conditions, in particular, injection velocity ratio (VR), have also been shown to influence both the susceptibility of the combustion chamber to combustion instabilities [8] and the contraction length of the LOx jet [9, 10]. The LOx jet contracts due to improved atomization and mixing which also reduces the length of the flame in the combustion chamber [7]. The influence of flame contraction on the combustion chamber speed-of-sound distribution has not yet been addressed in detail. Improving the understanding of how flame–acoustic interactions influences the speed-of-sound distribution is important for accurate tuning of acoustic resonance cavities and investigation of coupling of injector and combustion chamber resonance frequencies.

The combustor ‘H’ (BKH) is a rectangular combustion chamber used for the investigation of acoustic–flame interaction (Fig. 1). Combustion chamber acoustics can be externally forced producing high-amplitude pressure oscillations. The influence of these pressure oscillations on jet breakup and combustion zone length can be visualized through optical access windows located either side of the primary injection zone.

During investigation of acoustic dissipation, a frequency shift was observed during 1T-mode excitation, which manifested as an asymmetric amplitude response to a linear ramp of excitation frequency [11]. Examples of such asymmetric responses will be presented later in this paper (for example, in Fig. 4). In this work, the physical process leading to the frequency shift is investigated and

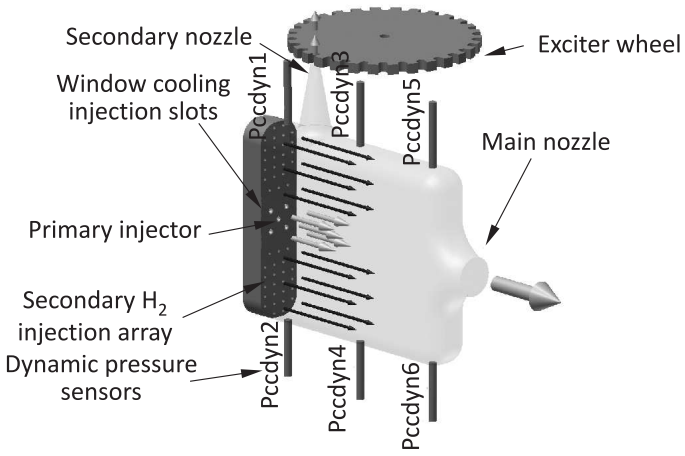


**Figure 1** Frequency of 1T eigenmode with on and off resonance excitation

a hypothesis is formed. Based on the hypothesis, a 1D model was developed to demonstrate the phenomena and to investigate the mechanism.

## 2 COMBUSTOR H

BKH is a rectangular combustion chamber designed to investigate flame–acoustic interactions. The combustion chamber (see Fig. 1) has a length of 305 mm, width of 50 mm, and a height of 200 mm. The rectangular cross section limits the fundamental modes of interest to two-dimensional form. The dimensions of length and height were chosen based on typical length and diameter of upper stage flight engines. This defines acoustic eigenmodes with representative frequencies, but the relatively high contraction ratio results in bulk flow Mach numbers an order of magnitude lower than those typical for real engines.

BKH has five primary shear-coaxial injection elements arranged in a matrix pattern and is operated with the propellant combination oxygen–hydrogen. Hydrogen is injected at either ambient (293 K) or cryogenic (60 K) temperature. The oxygen is injected at a cryogenic temperature of 120 K. Operating conditions are varied by varying the propellant mass flow rates and by using two different primary injector configurations (Fig. 2).

In addition to the primary injectors, secondary injection zones and window film cooling, both with ambient hydrogen, are employed in the operation of the combustion chamber. The secondary injection zones are used to limit recirculation above and below the primary injectors and to protect the combustion

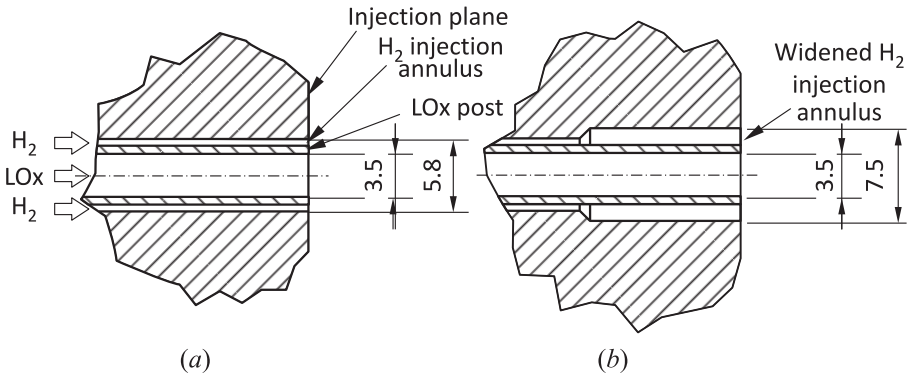


**Figure 2** Cross-sectional representations of the two primary injector configurations: ($a$) the nominal configuration; and ($b$) the slow configuration with a widened injector annulus. Dimensions are in millimeters

chamber and excitation system from thermal loads. The window cooling applies a thin film to protect the optical access windows from the central flame zone.

BKH is equipped with an excitation system. The excitation system excites combustion chamber acoustics by opening and closing a secondary nozzle perpendicular to the bulk flow direction. The secondary nozzle is open and closed by a rotating toothed wheel. The rate at which the wheel rotates controls the frequency of the excitation.

Acoustic pressure fluctuations are measured by the use of flush mounted Kistler type 6043A60 dynamic pressure sensors. The sensors have an accuracy of $\pm 1\%$, a dynamic range of $\pm 20$ bar and are sampled with a rate of 100 kHz. A 30-kilohertz antialiasing filter is applied to this signal.

## 3 PHYSICAL BASIS FOR ASYMMETRIC MODEL

### 3.1 Eigenmode Frequency Shift

A shift in eigenmodes frequencies was observed in a spectral analysis of the 1T and first combined longitudinal and transverse (1L1T) eigenmodes during excitation.

Figure 3 shows two power spectral density functions (PSDs), one during on-resonance excitation of the 1L1T mode and one during off-resonance excitation. A shift was observed in the first longitudinal (1L) mode, 1T, and 1L1T modes. The proximity of the excitation frequency to the 1L1T mode makes it difficult

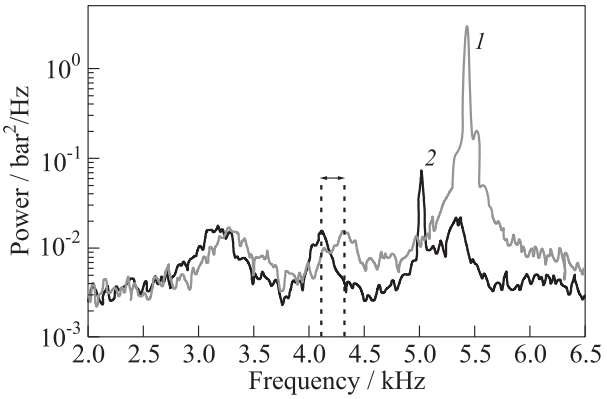


**Figure 3** Frequency of 1T mode with on (*1*) and off (*2*) resonance excitation of the 1L1T mode

to separate the influence of the frequency shift from the localized excitation. However, a clear shift of around 80 Hz was observed for the 1L mode and 200 Hz for the 1T mode.

The same phenomenon was observed in [12] when examining spectrograms of BKH excitation. The frequency shift of the 1L1T mode during 1T mode excitation was observed to be approximately 140 Hz. This is close to what is observable during 1L1T mode excitation in Fig. 3. The difference in frequency shifts between those observed in [12] and those presented here can be attributed to the spatial distribution of each eigenmode. Due to different spatial distributions, each eigenmode is influenced differently by changes in the speed-of-sound distribution.

In [12], the frequency increase of 140 Hz was estimated to correspond to an increase in bulk temperature of around 5.5%, or 62 K, which matched well with thermocouple measurements in the chamber wall. The increase in temperature was accompanied by an approximately 2% increase in $c^*$ combustion efficiency, both of which are postulated to result from improved atomization and mixing due to the transverse velocity component of the acoustic field acting on the primary injection zone.

### 3.2 Asymmetric Amplitude Response

To excite an eigenmode, BKH is exposed to a linear frequency ramp of an external acoustic driving force. During testing, an asymmetric response of the 1T mode to the linear frequency ramp was observed. Figure 4 shows a standard test sequence with an upwards and a downwards ramp through the 1T mode. During both

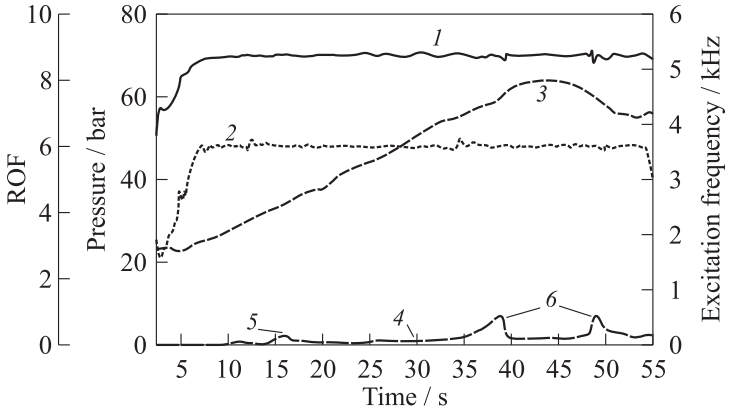


**Figure 4** BKH hot-fire test with up and down ramp of excitation frequency: *1* — combustion chamber pressure; *2* — ROF; *3* — excitation frequency; *4* — dynamic pressure amplitude; *5* — 1L-mode response (symmetric); and *6* — 1T-mode response (asymmetric)

the up and down ramp, the amplitude responses are asymmetric with a skew to higher frequencies (see Fig. 4).

If the asymmetry is due to changes in sound speed distribution, as suggested by the previous findings, the asymmetry is influenced by the energy density and distribution of the flame. Flame distribution and energy density in the near-injection region are influenced by the ratio of oxidiser-to-fuel (ROF), the injection conditions, and acoustic amplitude. Subsequently, the influence of operational and acoustic conditions on asymmetry was investigated. Figure 5 shows the influence of acoustic amplitude on the symmetry of amplitude response to a linear frequency ramp.

The following equation that describes a Fano profile was used to measure the asymmetry of the profile in this study:

$$L(\omega, A, \gamma, \omega_0, q) = A\left(\frac{(q + 2(\omega - \omega_0)^2/\Gamma)^2}{1 + (2(\omega - \omega_0)/\Gamma)^2}\right) \tag{1}$$

where $\Gamma$ is the full width at half maximum; $\omega$ is the given frequency; $\omega_0$ is the central frequency of the eigenmode; and the Fano symmetry coefficient $q$ is the measure of the profile symmetry [13]. The dependence of $q$ on acoustic amplitude is given in Fig. 5.

The Fano coefficient is inversely proportional and responds nonlinearly to the asymmetry. For high values of $q$, in this case over 100, the fit approaches a standard Lorentzian profile with no asymmetry. Values between 10 and 100 show low levels of asymmetry and as the value of $q$ approaches 1, the response

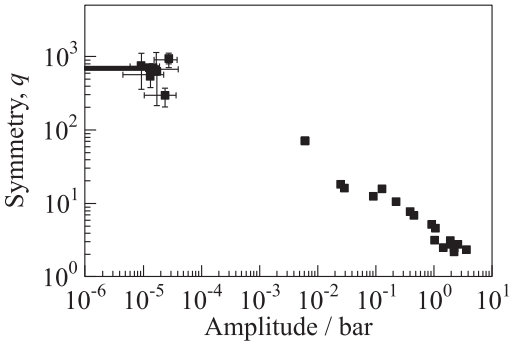


**Figure 5** Symmetry of the excited chamber response with increasing response amplitude (Pccdyn2 Fano coefficient)

becomes highly asymmetric. The response to pressure amplitude was found to be exponential and, so, Fig. 5 presents the relationship on double logarithmic axes.

The symmetry was strongly affected by pressure amplitude, with higher amplitudes decreasing the symmetry of the profiles. The response was linear on the double logarithmic axis. The uncertainty increased for higher $q$ values due to the decreasing sensitivity of $q$ for highly symmetric profiles.

Injection conditions, such as injection VR, influence the extent of the flame and interactions between the flame and pressure oscillations [8]. The influence of injection conditions on the amplitude response symmetry was investigated to examine the role of combustion in the frequency shift.

The symmetry was found to respond most consistently to changes in VR. Figure 6*a* shows the relationship between VR and symmetry, with decreasing VR leading to increased asymmetry. In oxygen–hydrogen combustion, the VR is known to influence the susceptibility of the LOx core to interaction with the acoustic field [9], and the pressure amplitude has been shown to strongly influence LOx core length and heat release distribution [12]. It should be noted that the result for VR in Fig. 6*a* cannot be isolated from the influences of ROF and hydrogen temperature, both of which also modify the VR in BKH, apart from the two primary injector configurations (see Fig. 2).

Considering the influence of hydrogen injection temperature in Fig. 6*b*, a higher asymmetry was generally observed in liquid hydrogen ($LH_2$) tests. However, there was a very large spread in asymmetry measured for gaseous hydrogen ($GH_2$) tests. The spread could be attributed to changes in primary hydrogen pressure drop, and an improved relationship with respect to pressure drop was observed (Fig. 6*c*). The asymmetry appeared to be less when the primary hydrogen pressure drop was above 10 bar and increased as pressure drop decreased toward zero.

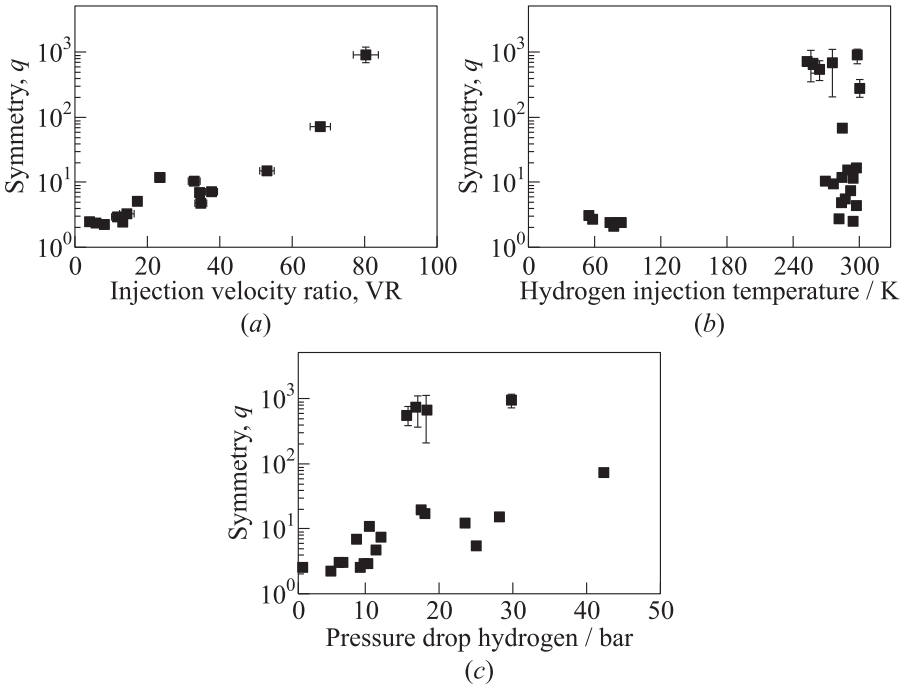


**Figure 6** Influence of injection conditions on amplitude response symmetry: (*a*) injection velocity ratio; (*b*) hydrogen injection temperature; and (*c*) hydrogen pressure drop (Pccdyn2 Fano coefficient)

### 3.3 Heat Release Distribution

In BKH, the response of the flame to both periodic and continuous excitation can be examined using OH* and visible imaging. The contraction of the LOx

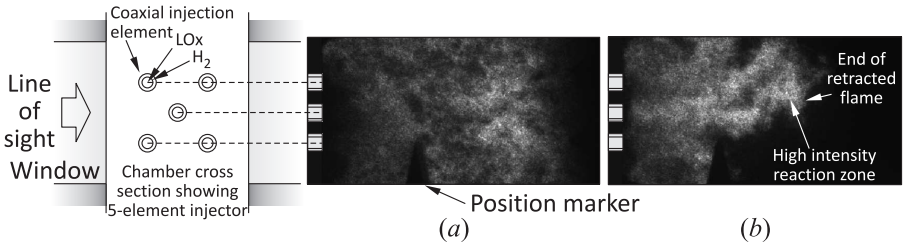


**Figure 7** Instantaneous OH* images for low acoustic pressure amplitude (off-resonance excitation) (*a*); and high 1T-mode amplitude (on-resonance excitation) (*b*)

core and the flame toward the faceplate during combustion instability has been well documented in a number of combustion chambers [7, 14, 15] and can also been observed in the OH* images in Fig. 7. The extent of this contraction has been shown to be dependent on operating conditions and on acoustic pressure amplitudes [7].

### 3.4 Hypothesis of Physical Mechanism

Based on the physical observations made in subsections 3.1–3.3, a hypothesis of the physical origin of the frequency shift was formed: when a linear frequency sweep is applied, the acoustic pressure amplitude increases as the eigenmode frequency is approached. The increasing amplitude causes a contraction of the flame toward the face plate, increasing the localised speed-of-sound. For the 1T mode, the change in speed of sound in the central region of the combustor results in an increase in eigenmode frequency. By this mechanism, the shift in frequency is proportional to the pressure amplitude.

An increase in eigenmode frequency means that the linear frequency sweep takes longer to reach the peak amplitude. In the approach to the eigenmode frequency, the excitation frequency is 'chasing' the eigenmode frequency. After the peak amplitude is reached, the pressure amplitude decreases and the flame returns to its undisturbed state which decreases the eigenmode frequency and subsequently causes a more rapid decrease in pressure amplitude as the distance between the forcing frequency and the eigenmode frequency increases more rapidly than the ramp rate.

This mechanism generates the unidirectional asymmetry observed with a skew only toward higher forcing frequencies. The strength of the skew is both dependent on amplitude and on a variable representing a relationship between contraction of the flame and a change in the speed of sound.

## 4 MODEL DESCRIPTION

A simple harmonic oscillator model capable of producing an eigenmode frequency shift based on acoustic pressure amplitude was developed based on the hypothesis presented in the previous section. This section describes the design of the model which is based on experimental observation.

### 4.1 Model Overview

The model implements a simple damped-driven harmonic oscillator with an input driving function and a feedback loop, based on pressure amplitude, to control

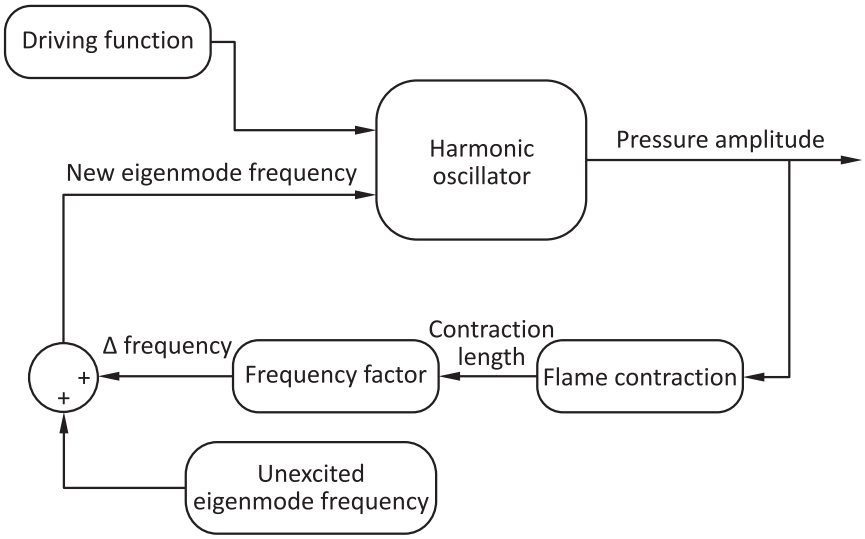


**Figure 8** Overview of frequency shift model

the eigenmode frequency. There are four key components to the model overview presented in Fig. 8:

(1) the driving function, which provides a linearly ramped sinusoidal chirp function to drive the harmonic oscillator;

(2) the 1D damped driven harmonic oscillator with a variable eigenmode frequency input, which calculates the pressure response;

(3) the flame contraction submodel, which implements the relationship between pressure amplitude and contraction length in Fig. 8; and

(4) a frequency factor submodel, which converts the contraction length into a change in the speed of sound.

The unexcited eigenmode frequency is supplied as a constant to the model. The driving function was chosen to ramp through an eigenmode frequency representative of the 1T mode in BKH. The ramp rate was the same as a typical BKH test (83.3 Hz/s). A sinusoid driving function was employed due to the simplicity of implementation. The damped-driven harmonic oscillator had a damping rate of 410 $s^{-1}$, which is representative of 1T mode damping rates observed in BKH [11]. The model is 1D and was implemented in Simulink. The model was run with a variable time step 4th-order Runge–Kutta integrator. Output sampling rate and calculation of passed variables were made at a constant time step of 10 $\mu$s.

### 4.2 Flame Contraction Model

The contraction of the flame toward the faceplate occurs when the combustion zone is exposed to high-amplitude pressure and velocity oscillations. A relationship between normalized acoustic amplitude ($P'/P_{cc}$) and oxygen core contraction length has been presented previously for BKH (Fig. 9) [15]. An approximately linear response with constant gradient was observed until pressure amplitude reaches around 5.5% of chamber pressure. After this, another approximately linear response with a much lower gradient was observed. The contraction of the flame is assumed to be represented by the contraction of the LOx core toward the faceplate. The relationships in Fig. 8 provide a physical basis for relating pressure amplitude to changes in speed-of-sound distribution through a change in heat-release distribution.

The flame contraction submodel links pressure amplitude with flame contraction length (Fig. 10). The input to the model is instantaneous pressure amplitude

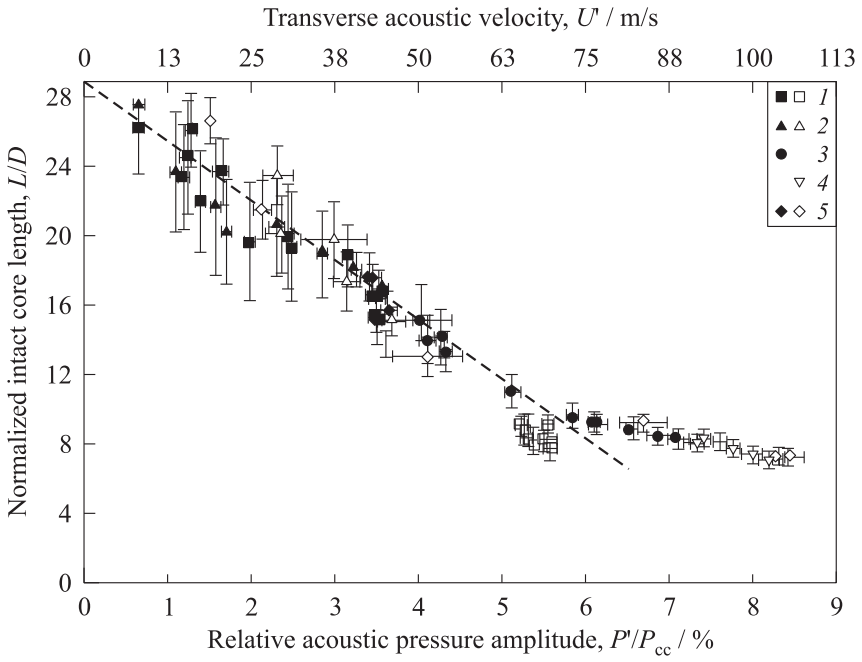


**Figure 9** Retraction of LOx core length due to increasing pressure amplitudes (modified from [7]): *1* — 60 bar; test A; *2* — 60 bar, text B; *3* — 60 bar, test C; *4* — 40 bar, test A; and *5* — 40 bar, test B. Filled signs refer to $GH_2$ and blank signs refer to $LH_2$. Line reflects the trend for all 60-bar $GH_2$ tests

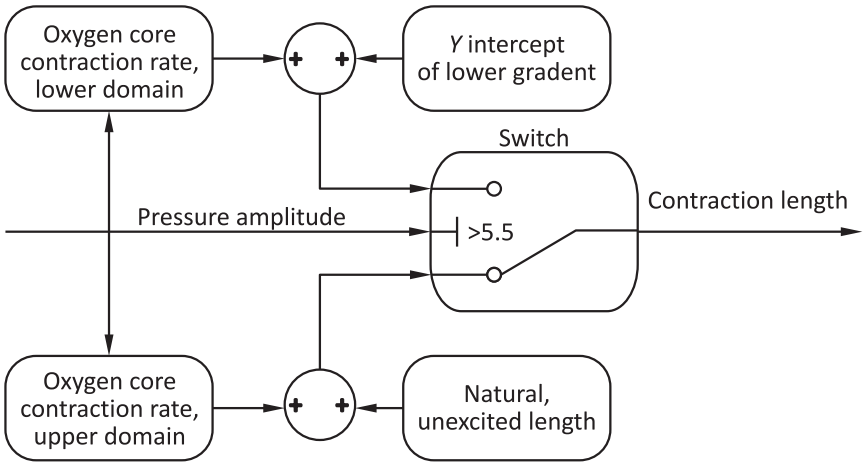


**Figure 10** Overview of flame contraction model

sampled at 10 $\mu$s. The model uses a switch to recreate the relationship observed in Fig. 9. Two domains were selected, an upper and a lower domain each applying a linear relationship with different coefficients of gradient and constants. The two domains were separated at the $P'/P_{cc}$ value of 5.5%. The model recreates this behavior using the input of the pressure amplitude to calculate the flame contraction for both domains before selection of the domain based on input pressure. The output of contraction length is used by the next model to calculate the frequency shift.

### 4.3 Frequency Shift Model

In Fig. 8, the contraction length is calculated in units of core length as a ratio to oxygen jet diameter. The heat release density and, therefore, the speed-of-sound and frequency shift are inversely proportional to the contraction of the oxygen core; so, the reciprocal of this value was taken as input.

The final step is to multiply the signal by a constant termed the 'frequency factor.' The frequency factor can be viewed as a compound constant consisting of three related physical phenomena. First, it represents the increase in energy density near the injection plane due to the contraction of the flame toward the faceplate. Second, the localized change in speed of sound due to the increased energy density. Third, the change in eigenmode frequency due to the localized change in speed-of-sound. This makeup of the frequency factor is illustrated in Fig. 11. In this simplified form, the parameter is different for each operating condition as the behavior of the flame is different for each operating condition.

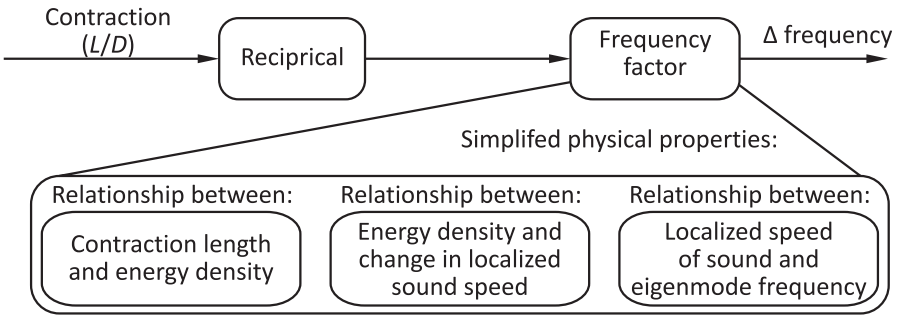


**Figure 11** Overview of frequency shift model

The influence of the frequency factor variable, along with the pressure amplitude, on signal asymmetry is investigated in the results section.

## 5 RESULTS

The influence of model parameters on the asymmetry and frequency shift was investigated and compared to test data. Two key parameters were investigated, the excitation amplitude and the frequency factor. The following subsection shows the influence of each of these parameters on the asymmetry of the signal response to excitation.

### 5.1 Recreation of Asymmetrical Response

The acoustic amplitude was varied whilst holding the frequency factor constant at 250. The response to a range of pressure amplitudes representative of those observed in BKH is presented in Fig. 12. When the pressure amplitude increases the asymmetry of the profile also increases. This demonstrates that the coupling between acoustic amplitude and asymmetric response in test data (see Fig. 5) is represented by the model (see Fig. 12). Additionally, a shift in eigenmode frequency is observed. The frequency shift was compared to test data for similar amplitudes and was found to be consistent. A more detailed comparison with experimental data, based on operating conditions, was not possible due to the simplification of the model parameters.

Figure 13 compares the amplitude with the asymmetry as measured by the fit of a Fano profile to the numerical model data. The asymmetry is represented by the Fano coefficient which is inversely proportional to the asymmetry and

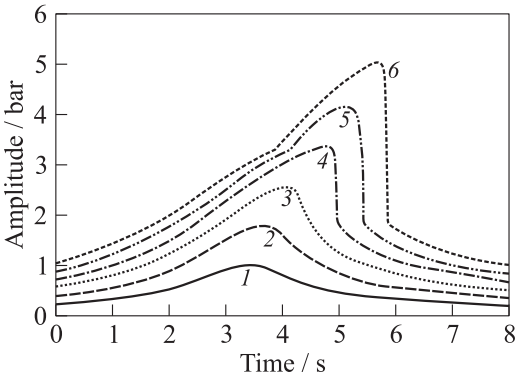


**Figure 12** Influence of amplitude parameter on assymetry: *1* — 1.00 bar; *2* — 1.75; *3* — 2.50; *4* — 3.25; *5* — 4.00; and *6* — 4.75 bar

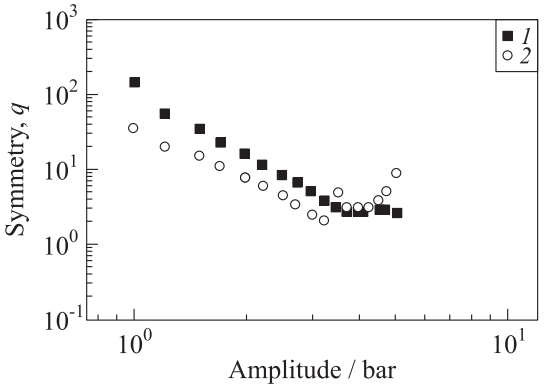


**Figure 13** Dependence of asymmetry on amplitude: *1* — frequency factor 200; and *2* — frequency factor 340

is nonlinear. The increasing asymmetry with pressure amplitude in Fig. 13 is reproduced by the model for two frequency factors, 200 and 340.

Two additional points need to be made. Two domains of operation are observed for the two frequency factors examined, an upper and a lower, each of which correspond to the two domains of LOx core contraction implemented in the model. In the lower amplitude region, a strong negative gradient is observed as the symmetry decreases with increasing amplitude. In the higher amplitude region, no gradient in the amplitude-symmetry relationship is observed. The lower gradient observed in the LOx core length $P'/P_{cc}$ relationship corresponds to the lower gradient region of the model response. The behavior of the sym-

metry coefficient, $q$, with respect to amplitude for a frequency factor of 340 is inconsistent with that of a frequency factor of 200. The increased frequency factor leads to larger asymmetries which are not accurately accounted for by the asymmetric Fano fitting profile when the amplitude is also high. This highlights a limitation in the application of Fano fitting profiles to asymmetric pressure response produced by a frequency shift.

### 5.2 Influence of Frequency Factor

The influence of the frequency factor was investigated for constant amplitude excitation. In Fig. 14, the amplitude was set to 3.3 bar. Increasing frequency factor enhances the asymmetry and the frequency shift due to the contraction of the flame. Frequency factors of up to 600 were investigated. However, frequency factors above 400 became increasingly nonrepresentative of the curves observed during testing.

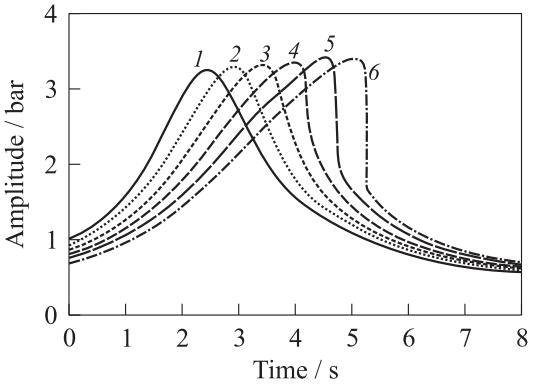


**Figure 14** Influence of frequency factor parameter on asymmetry: *1* — frequency factor = 0; *2* — 75; *3* — 150; *4* — 225; *5* — 300; and *6* — frequency factor = 375

### 5.3 Comparison with Test Data

The model was compared to test data to observe the response to both up and down ramping. Figure 15 shows the response of the model to up and down ramping overlaid on the up and down ramp presented in Fig. 4. Four curves are presented in each figure. Both the frequency ramps from test data and from the simulation are compared in black. In grey, the amplitude response of the model is given and compared to test data given by the frequency-amplitude scatter. For

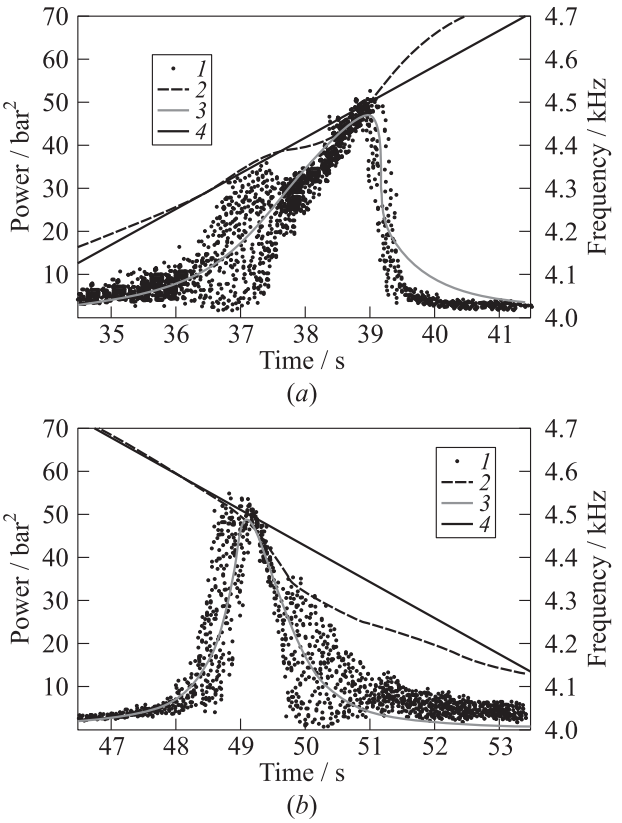


**Figure 15** Comparison of experimental (*1* and *2*) response data and computational (*3* and *4*) response for a positive frequency ramp (*a*) and a negative ramp (*b*): *1* — amplitude response; and *2* — frequency ramp

all tests, regions of high amplitude, low-frequency (LF) oscillations are observed when exciting near eigenmode frequencies. These regions show a large spread with respect to pressure vs. time and frequency plots. However, the average of this scatter matches closely the expected asymmetric response.

In general, the asymmetry observed in the simulation data agrees well with that of the test data. The skew is always shifted to higher frequencies as is observed in experimental data. The response of the model can be tuned using the amplitude and frequency factor variables to match the test data. In Fig. 15, the up and down ramps were tuned to improve the comparison with experimental data. The turning point matches well between the model and the test data. However, after passing the resonance, the profile does not follow the test data

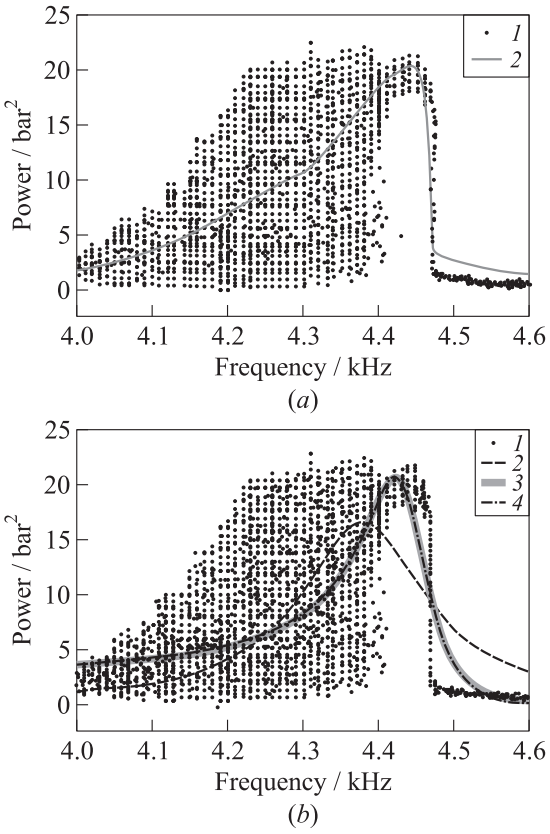


**Figure 16** Comparison of fit quality between 1D model (*a*) (*1* — experimental amplitude response; and *2* — computational amplitude response), and standard profiles (*b*) (*1* — dynamic pressure; *2* — Lorentzian profile; *3* — asymmetric Lorentzian profile; and *4* — Fano profile)

amplitude response optimally. This has been attributed to the nonlinearity in the test data ramp when compared to the perfect linear ramp of the model (see Fig. 15). Figure 16 shows a comparison with a highly asymmetric profile in the frequency domain which removes the influence of the deviation from a linear ramp observed in test data. The model showed good agreement with the asymmetry observed in test data.

The influence of white noise was tested by introducing an additional driving term into the model. The model was rerun to see if the noise had an impact on the turning point of the asymmetry or the ability of the model in general to match the experimental profile. White noise with amplitude of 10% of the

driving function amplitude was found to have no influence in the ability of the model to recreate the phenomena observed in experimental data.

The response of the frequency shift model was compared to three response profiles, the Fano profile, which has been described in Eq. (1), the Lorenzian profile and the asymmetric Lorentzian profile which are described by the following equations:

$$L(\omega, A, \alpha, \omega_0) = A\left(\frac{\alpha^2}{(\omega-\omega_0)^2+\alpha^2}\right); \tag{2}$$

$$L(\omega, A, \alpha, \omega_0, B) = A\left(\frac{1+B((\omega-\omega_0)/\alpha)^2+B^2}{1+((\omega-\omega_0)/\alpha)^2}\right) \tag{3}$$

where $\alpha$ is the half width at half maximum and $B$, for the asymmetric Lorentzian profile, is the asymmetry. Both the Fano and asymmetric Lorentzian profiles can take into account asymmetry with the coefficient $q$ for the Fano profile and $B$ for the asymmetric Lorentzian profile. For the asymmetric Lorentzian profile, the value of $B$ varies between $-1$ and 1 with $B = 0$ reducing to the Lorentzian profile without symmetry. The asymmetric Lorentzain profile is typically used in investigation of helioseismology and a more detailed description of its applications in that field is given in [16]. The Lorentzian profile without asymmetry cannot take this into account and, as a consequence, can poorly fit asymmetric profiles [11]. Figure 16 shows the comparison between the response of the frequency shift model and the three profiles described by Eqs. (1)–(3).

The quality of the fit using the frequency shift model is improved with respect to the asymmetric profiles used previously for measurement of acoustic dissipation. When comparing the different models directly, the frequency shift model fits the test data the most closely. The asymmetric profiles offer an improved fit over the symmetric Lorentzian profile, especially for amplitudes above 1/3 of peak amplitude, but do not capture the physical behavior of the asymmetry.

## 6 DISCUSSION

Understanding and prediction of eigenmode frequency shift under representative conditions are important for limiting the risk of combustion instabilities. The frequency shift observed in test data is well explained by a change in speed-of-sound distribution due to contraction of the flame. Contraction of the flame due to improved breakup and mixing processes through exposure to transverse acoustic oscillations has previously been observed in BKH [15]. A contracting flame mechanism is consistent with the dependency of asymmetry on injection conditions, in particular, to VR which has been shown to influence the susceptibility of LOx core breakup to combustion instabilities [9, 10].

The model presented here shows that the frequency shift model can account for the observations made in test data. However, due to the simplified nature of the model, it is limited when applied to different systems and taking into account complex processes such as the influence of injection conditions.

The two active blocks that relate acoustic amplitude with frequency shift, the flame contraction model and the frequency shift model, are significant simplifications on the processes they represent. For example, the contraction rate of the jet with respect to the pressure amplitude is dependent on operating conditions and geometry. In BKH, this is represented by the influence of VR on asymmetry. The model presented here is tuned for use in BKH by utilizing existing results of LOx core breakup. No data exist where the relationship of amplitude and LOx core contraction can be examined under representative conditions for cases outside of BKH. A more generalized relationship between acoustic amplitude, LOx core contraction, and injection conditions (such as VR) would help in further development of this model.

The second parameter used to relate pressure amplitude to eigenmode frequency shift is the frequency factor. The frequency factor relates the contraction of the jet to the change in sound speed and frequency. The parameter is a simplification of a complex set of relationships that are dependent on operating condition and propellant type. For example, if the same contraction occurred in a methane flame would the subsequent speed-of-sound increase be the same? This is unlikely as the propellant combinations have different combustion temperatures and combustion products. For the model to be generalized and maintain accuracy, the incorporation of additional terms into the frequency factor block would be required.

The distribution of the flame is restricted to the central axis of the combustor in BKH and is a specialized case. Above and below the flame zone, secondary hydrogen dominates and in these zones, the speed-of-sound is not influenced by contraction of the flame. In real engines, combustion is distributed across the entire cross section. This could lead to a larger frequency shift if the entire flame zone was to retract. The height of the BKH combustion chamber is comparable with upper stage engines. However, the flame occupies approximately one quarter of this region, restricting the response to only this region.

The model accurately reproduced the influence of amplitude on asymmetry over a limited amplitude domain. The inconsistency observed between numerical and experimental results was attributed to the ability of the asymmetric fitting functions to capture highly asymmetric profiles of this type. This is highlighted in Fig. 16. The Fano and asymmetric Lorentzian profiles provide a better fit than the symmetric Lorentzian profile but are significantly worse than the frequency shift model at following the experimentally obtained response. This suggests that the Fano and asymmetric Lorentzian profiles should only be used as tools to improve the accuracy of the measurement of response peak width, and that

they are not physically representative of the amplitude, flame contraction, and speed-of-sound interactions.

With further refinement, the model could be used to tune acoustic resonators to resonance modes under unstable conditions. Additionally, the model could be used to investigate the natural limit cycle of injector-resonance coupling where a shift in chamber mode frequency shifts the chamber in and out of resonance with the injector. To accurately measure this in one dimension, the model would have to have a frequency dependent driving amplitude which will be implemented in future developments of the model.

## 7 CONCLUDING REMARKS

In experiments with combustor 'H,' an increase in combustion chamber eigenmode frequencies was observed during excitation of eigenmodes with a transverse velocity component. The frequency shift was observed as an asymmetric amplitude response to a linear excitation ramp. Acoustic amplitude and operating conditions influenced the strength of the asymmetry. This led to the hypothesis that a contraction of the flame and the subsequent increase in temperature in the near faceplate region was the physical cause of the observed frequency shift in transverse modes.

To test the hypothesis, a 1D damped-driven harmonic oscillator model was developed. The model included a frequency shift term with the amount of shift being related to the instantaneous acoustic amplitude. When exposed to a linear frequency sweep, the acoustic model was found to accurately follow the asymmetries observed in test data. Two parameters, contraction length dependent on acoustic amplitude and a frequency factor, were incorporated into the model to influence the asymmetry. A parametric study of each of the parameters showed that the dependence of asymmetry on amplitude observed in test data was also reproduced by the acoustic model. The frequency factor can be tuned to account for the influence of operating condition and combustion chamber configuration. However, this tuning is currently dependent on the use of experimental data and generalized applicability of the model would first require the development of appropriate submodels to account for other operating conditions and configurations.

This model is the first step in understanding the importance of acoustic sound speed distribution on combustion instability. The model is of particular relevance for tuning of acoustic resonators which have high sensitivity to acoustic frequency. Additionally, injection coupling is highly sensitive to the eigenmode frequencies of the combustion chamber and the injector. A slight shift in eigenmode frequency may mean the difference between stable or unstable operation. Further development of the model is required to generalize the results and allow

its use in the study of the frequency sensitivity of injection-coupled instabilities.

## ACKNOWLEDGMENTS

The authors would like to thank the P8 test team for their effort and contribution to test operations, as well as the DLR optical team for setting up and operation of optical diagnostics. Additional thanks to Marco Anderer for his contribution to the development and testing of the Simulink numerical model. This work has been conducted in association with the Franco-German REST cooperation (Rocket Engine Stability iniTiative).

## REFERENCES

1. Harrje, D. T., and F. H. Reardon. 1972. *Liquid propellant rocket combustion instability*. Washington, D.C.: NASA. 657 p.
2. Yang, V., and W. Anderson, eds. 1995. *Liquid rocket engine combustion instability*. Progress in astronautics and aeronautics ser. Washington, D.C.: AIAA. Vol. 169. 657 p.
3. Heidmann, M. F., and P. R. Wieber. 1966. Analysis of frequency response characteristics of propellant vaporization. Lewis Research Centre, National Aeronautics and Space Administration. NASA TN D-3749.
4. Hardi, J., M. Oschwald, and B. Dally. 2013. Acoustic characterisation of a rectangular rocket combustor with liquid oxygen and hydrogen propellants. *J. Aerosp. Eng.* 227:436–446.
5. Gröning, S., D. Suslov, M. Oschwald, and T. Sattelmayer. 2013. Stability behaviour of a cylindrical rocket engine combustion chamber operated with liquid hydrogen and liquid oxygen. *5th European Conference for Aerospace Sciences (EUCASS)*.
6. Kaess, R., S. Koeglmeier, R. Behr, B. Kniesner, and T. Sattelmayer. 2013. Impact of axial gradient on combustion chamber acoustics. *5th European Conference for Aerospace Sciences (EUCASS)*.
7. Hardi, J., H. C. Gomez Martinez, M. Oschwald, and D. Bassam. 2014. LOx jet atomization under transverse acoustic oscillations. *J. Propul. Power* 30(2):337–349.
8. Wanhainen, J. P., H. C. Parish, and E. W. Conrad. 1966. Effect of propellant injection velocity on screech in 20 000-pound hydrogen–oxygen rocket engine. NASA TN D3373.
9. Davis, D., and B. Chehroudi. 2006. Shear-coaxial jets from a rocket-like injector in a transverse acoustic field at high pressures. *44th AIAA Aerospace Sciences Meeting and Exhibit*. Reno, Nevada.
10. Davis D., and B. Chehroudi. 2007. Measurements in an acoustically driven coaxial jet under sub-, near-, and supercritical conditions. *J. Propul. Power* 23(2):364–374.

11. Webster, S., J. Hardi, and M. Oschwald. 2014. Analysis of acoustic energy dissipation in a rectangular combustion chamber with injection of cryogenic propellants. *Space Propulsion Conference and Exhibit*.
12. Hardi, J. 2012. Experimental investigation of high frequency combustion instability in cryogenic oxygen–hydrogen rocket engines. The University of Adelaide. PhD Thesis.
13. Fano, U. 1961. Effects of configuration interaction on intensities and phase shifts. *Phys. Rev.* 124(6):1866–1878.
14. Woodward, R. D., P. Sibtosh, F. Shahram, and R. J. Santoro 2006. LOx/$GH_2$ shear coaxial injector atomization studies at large momentum flux ratios. *42nd AIAA/ASME/SAE/ASEE Joint Propulsion Conference*.
15. Yang, B., F. Cuoco, and M. Oschwald. 2007. Atomization and flames in LOx/$H_2$- and LOx/$CH_4$-spray combustion. *J. Propul. Power* 23(4):763–772.
16. Toutain, T., T. Appourchaux, C. Fröhlich, A. G. Kosovichev, R. Nigam, and P. Scherrer. 1998. Asymmetry and frequencies of low-degree p-modes and the structure of the Sun's core. *Astrophys. J.* 506:L147–L150.